Journal of Biomechanics 85 (2019) 101–107

Contents lists available at ScienceDirect

Journal of Biomechanics

journal homepage: www.elsevier.com/locate/jbiomech
www.JBiomech.com

Stiffness modulation of redundant musculoskeletal systems

Dimitar Stanev, Konstantinos Moustakas

Department of Electrical and Computer Engineering, University of Patras, Greece

ARTICLE INFO

Article history:
Accepted 8 January 2019

Keywords:
Stiffness
Musculoskeletal systems
Mixed dynamics

ABSTRACT

This work presents a framework for computing the limbs' stiffness using inverse methods that account for the musculoskeletal redundancy effects. The musculoskeletal task, joint and muscle stiffness are regulated by the central nervous system towards improving stability and interaction with the environment during movement. Many pathological conditions, such as Parkinson's disease, result in increased rigidity due to elevated muscle tone in antagonist muscle pairs, therefore the stiffness is an important quantity that can provide valuable information during the analysis phase. Musculoskeletal redundancy poses significant challenges in obtaining accurate stiffness results without introducing critical modeling assumptions. Currently, model-based estimation of stiffness relies on some objective criterion to deal with muscle redundancy, which, however, cannot be assumed to hold in every context. To alleviate this source of error, our approach explores the entire space of possible solutions that satisfy the action and the physiological muscle constraints. Using the notion of null space, the proposed framework rigorously accounts for the effect of muscle redundancy in the computation of the feasible stiffness characteristics. To confirm this, comprehensive case studies on hand movement and gait are provided, where the feasible endpoint and joint stiffness is evaluated. Notably, this process enables the estimation of stiffness distribution over the range of motion and aids in further investigation of factors affecting the capacity of the system to modulate its stiffness. Such knowledge can significantly improve modeling by providing a holistic overview of dynamic quantities related to the human musculoskeletal system, despite its inherent redundancy.

1. Introduction

The regulation of the limbs' stiffness by the Central Nervous System (CNS) has been subject to many studies over the past decades (Hogan, 1981; Flash and Hogan, 1985; Flash, 1987; Flash and Mussa-Ivaldi, 1990; Perreault et al., 2001; Babikian et al., 2015). Intuitively, stiffness (or rigidity) is the extent to which the limbs resist movement induced by external forces. In this work, task[1] (e.g., endpoint stiffness), joint and muscle stiffness are distinguished and their relationship is studied. Since muscles are the main actors in musculoskeletal systems, their co-contraction affects the joint and task stiffness (Kutch and Valero-Cuevas, 2011; Inouye and Valero-Cuevas, 2016). Due to the redundancy of actuators, there exist infinitely many solutions for muscle forces giving rise to the same movement. It is thus important to consider not only the motion of the limbs, but also the degrees of muscle co-contraction.

Musculoskeletal systems are intrinsically redundant (Bernshtein, 1967), i.e., there are more Degrees of Freedom (DoFs) than those required to perform certain tasks (kinematic redundancy) and each DoF is actuated by multiple muscles (dynamic redundancy). This poses numerous challenges in modeling and simulation and as a result, it has been pointed out that many common approaches are oversimplified (Valero-Cuevas et al., 2009). This, although deliberate since it simplifies the mathematical implementation and analysis, may also negatively affect the validity of these models and the obtained results (Wesseling et al., 2015) (e.g., estimation of muscle forces, joint reaction loads and stiffness characteristics). Minimum effort solutions (e.g., activation squared) tend to underestimate muscle co-contraction, since co-contraction has by construction zero net joint effect, rendering it unsuitable in applications where this assumption may not hold (Pedotti et al., 1978; Prilutsky and Zatsiorsky, 2002; Koeppen et al., 2017). Therefore, appropriate methods need to be developed for finding the possible system realizations and further classifying strategies available to the CNS.

Experimental methods for measuring the endpoint stiffness have been proposed and used in conjunction with model-based

E-mail addresses: stanev@ece.upatras.gr (D. Stanev), moustakas@upatras.gr (K. Moustakas)

[1] The use of endpoint instead of task stiffness would lead to a more intuitive presentation, however, we can compute the stiffness of any point on the model, thus a more general term of "task" stiffness is adopted.

https://doi.org/10.1016/j.jbiomech.2019.01.017
0021-9290/

estimates in order to study the effect of muscle co-contraction on it (Mussa-Ivaldi et al., 1985; Flash and Mussa-Ivaldi, 1990). Model-based estimation of joint and task stiffness requires the assessment of muscle forces, which can be obtained either from Electromyography (EMG) recordings or by minimizing some objective criterion, such as minimum effort. However, both approaches have their drawbacks, namely not all muscles are easily accessible in practice (e.g., deep muscles), transformation from EMG to muscle force is inexact and optimization assumptions do not always hold. The authors in (Hu et al., 2011) compared the experimentally measured endpoint stiffness against the model-based estimates, concluding that deviations from their predictions can be explained by muscle redundancy. To overcome these limitations, a method for identifying all possible solutions of muscle forces that satisfy the task as well as physiological muscle constraints is proposed, in order to evaluate their influence on the task and joint space stiffness.

The main contribution of this work is the calculation of the feasible task and joint stiffness in the context of an arbitrary action, by modeling musculoskeletal redundancy using the notion of null space. In Section 2.1, the relationship between muscle, joint and task space stiffness is presented, while in Section 2.2, a method for describing the feasible muscle forces is introduced, enabling the calculation of the feasible stiffness. The feasible endpoint stiffness of a simplified arm model performing a hand movement and the joint stiffness of a realistic gait model are studied in Sections 3.1 and 3.2, respectively. These case studies highlight the assumption-free nature of the proposed framework, which therefore is able to recover the entire stiffness space.

2. Methods

2.1. Muscle, joint and task space stiffness

In this section, we will present a short overview of the mathematical definitions for calculating the muscle, joint and task space stiffness as outlined by previous studies (Hogan, 1981; Flash and Hogan, 1985; Flash, 1987; Perreault et al., 2001; Inouye and Valero-Cuevas, 2016), while a more detailed presentation can be found in Supplementary materials. In the following section, we will introduce a method for calculating the feasible muscle forces that satisfy the motion and the physiological muscle constraints. As the muscles are the main actors of the system, it is important to examine the effect of muscle redundancy on the calculation of limbs' stiffness.

The muscle stiffness is defined as

$$\boldsymbol{K}_m = \frac{\partial \boldsymbol{f}_m}{\partial \boldsymbol{l}_m},\ \boldsymbol{K}_m \in \Re^{m\times m} \tag{1}$$

where $\boldsymbol{f}_m \in \Re^m$ represents the muscle forces, $\boldsymbol{l}_m \in \Re^m$ the musculotendon lengths and m the number of muscles. The joint stiffness is defined as

$$\boldsymbol{K}_j = \frac{\partial \boldsymbol{\tau}}{\partial \boldsymbol{q}},\ \boldsymbol{K}_j \in \Re^{n\times n} \tag{2}$$

where $\boldsymbol{\tau} \in \Re^n$, $\boldsymbol{q} \in \Re^n$ are the generalized forces and coordinates, respectively and n the DoFs of the system. Finally, the task stiffness is defined as

$$\boldsymbol{K}_t = \frac{\partial \boldsymbol{f}_t}{\partial \boldsymbol{x}_t},\ \boldsymbol{K}_t \in \Re^{d\times d} \tag{3}$$

where $\boldsymbol{f}_t \in \Re^d$ denotes the forces, $\boldsymbol{x}_t \in \Re^d$ the positions and d the DoFs of the task.

The derivation starts with a model for computing the muscle stiffness matrix $\boldsymbol{K}_m$. The two most adopted approaches are to either use the force-length characteristics of the muscle model or to approximate it using the definition of the short range stiffness, where the latter is shown to explain most of the variance in the experimental measurements (Hu et al., 2011). The short range stiffness is proportional to the force developed by the muscle (f_m)

$$k_s = \gamma \frac{f_m}{l_m^o} \tag{4}$$

where $\gamma = 23.4$ is an experimentally determined constant (Cui et al., 2008) and l_m^o the optimal muscle length. This definition will be used to populate the diagonal elements of the muscle stiffness matrix, whereas inter-muscle coupling (non-diagonal elements) will be assumed zero since it is difficult to measure and model in practice.

The joint stiffness is related to the muscle stiffness through the following relationship

$$\boldsymbol{K}_j = -\frac{\partial \boldsymbol{R}^T}{\partial \boldsymbol{q}} \bullet_2 \boldsymbol{f}_m - \boldsymbol{R}^T \boldsymbol{K}_m \boldsymbol{R} \tag{5}$$

where the first term captures the varying effect of the muscle moment arm ($\boldsymbol{R} \in \Re^{m\times n}$), while the second term maps the muscle space stiffness to joint space. The notation $\bullet_2$ (Supplementary materials) denotes a product of a rank-3 tensor ($\frac{\partial \boldsymbol{R}^T}{\partial \boldsymbol{q}} \in \Re^{n\times m\times n}$, a 3D matrix) and a rank-1 tensor ($\boldsymbol{f}_m \in \Re^m$, a vector), where the index 2 specifies that the tensor dimensional reduction (by summation) is performed across the second dimension, resulting in a reduced rank-2 tensor of dimensions $n \times n$ (Kolda and Bader, 2009).

In a similar manner, the task stiffness is related to the muscle stiffness through the following relationship

$$\boldsymbol{K}_t = -\boldsymbol{J}_t^{+T}\left(\frac{\partial \boldsymbol{J}_t^T}{\partial \boldsymbol{q}} \bullet_2 \boldsymbol{f}_t + \frac{\partial \boldsymbol{R}^T}{\partial \boldsymbol{q}} \bullet_2 \boldsymbol{f}_m + \boldsymbol{R}^T \boldsymbol{K}_m \boldsymbol{R}\right)\boldsymbol{J}_t^{+} \tag{6}$$

where the task Jacobian matrix ($\boldsymbol{J}_t \in \Re^{d\times n}$) describes the mapping from joint to task space ($\Re^n \to \Re^d$), $+$ stands for the Moore-Penrose pseudoinverse and $+T$ the transposed pseudoinverse operator.

2.2. The influence of musculoskeletal redundancy

In this section, we propose a method for identifying the feasible muscle forces that satisfy the movement and the physiological muscle constraints. This method does not assume minimization of some objective criterion, but relies solely on the movement context, the muscle model (e.g., linear/nonlinear muscle model and synergy encoding) and the anatomical properties of the muscle routing (the muscle moment arm and its null space). The family of solutions is guaranteed to preserve the system's kinematic behavior, i.e., produce the same movement, corresponding to different levels of muscle co-activation.

In a typical experimental setup the motion and externally applied forces are recorded. Given these recordings, Inverse Kinematics (IK) and Inverse Dynamics (ID) are performed in order to assess the model kinematics and kinetics that satisfy the experimental measurements (Erdemir et al., 2007). Instead of estimating the muscle forces using Static Optimization (SO) or some other method (Anderson and Pandy, 2001; Thelen and Anderson, 2006), we can solve $\boldsymbol{\tau} = -\boldsymbol{R}^T \boldsymbol{f}_m$ for $\boldsymbol{f}_m$ accounting for the null space muscle forces, which are present only when projecting from low- to high-dimensional space. More formally, the muscle forces $\boldsymbol{f}_m$ can be expressed as the sum of two mutually orthogonal subspaces (Stanev and Moustakas, 2019), spanning the column ($f_m^{\parallel} \in \mathbb{C}(R^{+T})$) and null space ($f_m^{\perp} \in \mathbb{N}(R^{+})$), respectively

$$\boldsymbol{f}_m = \boldsymbol{f}_m^{\parallel} + \boldsymbol{f}_m^{\perp} = -\boldsymbol{R}^{+T}\boldsymbol{\tau} + \boldsymbol{N}_{\boldsymbol{T}_R}\boldsymbol{f}_{m0},\ \boldsymbol{N}_{\boldsymbol{T}_R} = \boldsymbol{I} - \boldsymbol{R}\boldsymbol{R}^{+} \tag{7}$$

where $\boldsymbol{N}_{\boldsymbol{T_R}} \in \Re^{m\times m}$ is the moment arm null space projection operator and $\boldsymbol{f}_{m0} \in \Re^m$ a vector of arbitrarily selected null space muscle forces. Note that this definition spans the entire $\Re^m$ for some arbitrary value of $\boldsymbol{\tau}$, whereas in reality muscle forces are strictly positive (contraction) and bounded (limited force). Therefore, in general, this solution may not be physiologically correct (namely $\exists i : f_m^i > f_{\max}^i$ or $f_m^i < 0$). However, the null space term $\boldsymbol{f}_m^{\perp}$ can provide a suitable correction in order to satisfy the physiological constraints of the muscles. In this study, we will assume a linear muscle model, such as that the force is proportional to the strength and activation level of the muscle

$$\boldsymbol{f}_m = \boldsymbol{f}_{\max} \circ \boldsymbol{a}_m,\ \boldsymbol{0} \preceq \boldsymbol{a}_m \preceq \boldsymbol{1} \tag{8}$$

where $\boldsymbol{a}_m \in \Re^m$ represents a vector of muscle activations, $\boldsymbol{f}_{\max} \in \Re^m$ a vector specifying the maximum muscle force and $\circ$ the Hadamard (elementwise) product[2]. We can impose bounds on the possible solutions of $\boldsymbol{f}_{m0}$ in the form of linear inequalities, by noting that Eqs. (7) and (8) must be equal

$$\begin{aligned} f_{\max} \circ a_m = f_m^{\parallel} + N_{T_R} f_{m0},\ 0 \le a_m \le 1 \rightarrow \\ \left[\begin{array}{c} -N_{T_R} \\ \hdashline N_{T_R} \end{array}\right] f_{m0} \le \left[\begin{array}{c} f_m^{\parallel} \\ \hdashline f_{\max} - f_m^{\parallel} \end{array}\right] \\ Z f_{m0} \le \beta. \end{aligned} \tag{9}$$

An important advantage of this formulation is that different muscle models can be included in the derivation of the feasible inequality. For example, we can incorporate muscle synergies (Steele et al., 2015) by substituting $\boldsymbol{a}_m = \boldsymbol{W}\boldsymbol{c}$ in Eq. (9). Term $\boldsymbol{W} \in \Re^{m\times s}$ represents the muscle synergy matrix and $\boldsymbol{c} \in \Re^s$ the synergy activations. Moreover, Eq. (9) defines a closed and convex space for $\boldsymbol{f}_{m0}$ (Supplementary materials), which can therefore be sampled using vector enumeration techniques (Avis and Fukuda, 1992; Vempala, 2005). Finally, the feasible muscle force set is computed as the sum of the particular solution and the null space forces that satisfy Eq. (9)

$$\boldsymbol{f}_m^{\oplus} = \left\{\boldsymbol{f}_m^{\parallel} + \boldsymbol{N}_{\boldsymbol{T_R}}\boldsymbol{f}_{m0}^i,\ \forall i\right\}. \tag{10}$$

In order to compute the feasible muscle force set $\boldsymbol{f}_m^{\oplus}$, the physiological null space muscle forces $\boldsymbol{f}_{m0}$ must be obtained by sampling the space defined by a set of linear inequalities (Eq. (9)). The linear inequalities define a closed polytope (a convex polyhedron) as an intersection of a finite number of half-spaces (hyperplane- or H-representation). The conversion from H-representation to V-representation is called vertex enumeration and can be achieved by using either a deterministic or randomized approach. From an arrangement of n hyperplanes in $\Re^d$, v vertices are determined in $O(n^2 d v)$ time. We used the `lrs` library (Avis and Fukuda, 1992), which provides a self-contained ANSI C implementation of the reverse search algorithm for vertex enumeration. After obtaining the extreme points of the polytope, additional solutions are generated by interpolating ($\boldsymbol{\psi} = \lambda\boldsymbol{x} + (1-\lambda)\boldsymbol{y}$) between vertices. This process generates samples spanning the entire polytope due to its convexity.

3. Results

We will present two case studies, where the influence of musculoskeletal redundancy on the feasible task and joint stiffness will be evaluated. In the first case, a simplified planar arm model

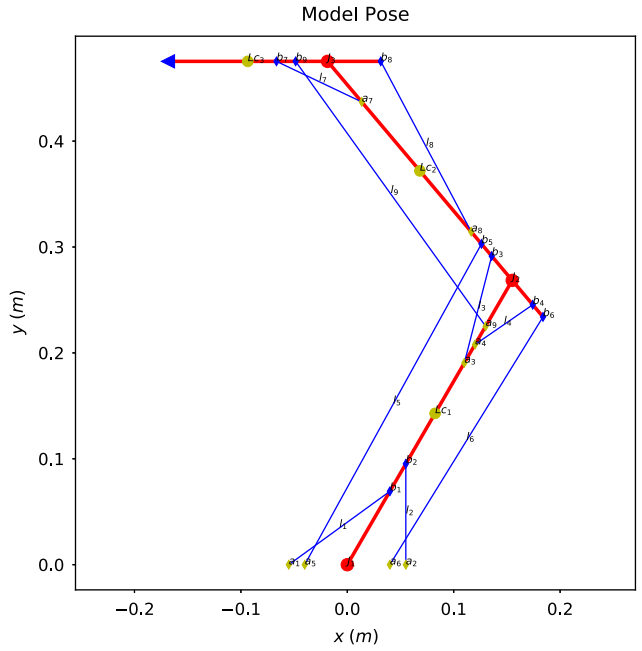

Fig. 1. Diagram of the simplified arm model with three DoFs and nine muscles, some of them being bi-articular. The muscle origins are labeled as a_i and the muscle insertions as b_i. l_i stands for muscle length, Lc_i for center of mass and J_i for joint center.

(Fig. 1), having three DoFs and nine muscles, is appropriately constructed to demonstrate both kinematic and dynamic redundancy (i.e., $d < n < m$). The movement will be planned in task space by controlling the position of the hand using task space projection (Stanev and Moustakas, 2018). In the second experiment, the feasible joint stiffness of the hip, knee and ankle joints during walking will be assessed using the `OpenSim` (Delp et al., 2007) gait model that has ten DoFs and eighteen muscles (Millard et al., 2013). These models were constructed with an emphasis on clarity, simultaneously preserving a degree of anatomic realism.

3.1. Variability in the arm endpoint stiffness

In this experiment, the feasible task and joint stiffness of a simplified arm model will be evaluated. More specifically, Eqs. (5) and (6) will be used to compute the stiffness at each time step of the simulation. Since stiffness depends on the muscle forces and the model is redundant, there are infinitely many solutions that satisfy the reaching task. To account for this, the space defined by Eq. (9) will be sampled in order to compute the feasible muscle forces (Eq. (10)), assuming a linear muscle model. Consequently, these solutions will be used to obtain the feasible stiffness values.

Since task forces $\boldsymbol{f}_t$ are required in the calculation of Eq. (9), the planning can be encoded using task space projection (Khatib et al., 2009; Stanev and Moustakas, 2018), by tracking the desired position of the end effector. Essentially, a mixed dynamics scheme is adopted, where the task space ID model-based controller accepts the desired task goal and returns the generalized forces $\boldsymbol{\tau}$. These forces are applied to the model in a Forward Dynamics (FD) manner and the resulting movement is thus simulated. Furthermore, the generalized forces are used to evaluate the particular solution $\boldsymbol{f}_m^{\parallel}$ (Eq. (7)), required in the calculation of the feasible muscle forces. A Proportional Derivative (PD) tracking scheme is adopted

$$\ddot{\boldsymbol{x}}_t = \ddot{\boldsymbol{x}}_d + k_p(\boldsymbol{x}_d - \boldsymbol{x}_t) + k_d(\dot{\boldsymbol{x}}_d - \boldsymbol{x}_t) \tag{11}$$

where $\boldsymbol{x}_d$, $\dot{\boldsymbol{x}}_d$, $\ddot{\boldsymbol{x}}_d$ are the desired position, velocity and acceleration of the task and $k_p = 50$, $k_d = 5$ the tracking gains. The desired task

[2] Elementwise multiplication is preferred in comparison to the traditional matrix vector approach (e.g, $\boldsymbol{f}_m = \boldsymbol{F}_{\max}\boldsymbol{a}_m$) to explore the fact that $\boldsymbol{F}_{\max}$ is a diagonal matrix.

goal is derived from a smooth sigmoid function that produces bell-shaped velocity profiles in any direction around the initial position of the end effector

$$\begin{aligned} \boldsymbol{x}_d(t) &= \left[x_t(0) + \tfrac{a}{2}(\tanh(b(t-t_0))+1),\ y_t(0)\right]^T \\ \dot{\boldsymbol{x}}_d(t) &= \tfrac{d\boldsymbol{x}_d(t)}{dt},\ \ddot{\boldsymbol{x}}_d(t) = \tfrac{d\dot{\boldsymbol{x}}_d(t)}{dt} \\ \boldsymbol{x}'_d &= \boldsymbol{H}_z(\gamma)\boldsymbol{x}_d,\ \dot{\boldsymbol{x}}'_d = \boldsymbol{H}_z(\gamma)\dot{\boldsymbol{x}}_d,\ \ddot{\boldsymbol{x}}'_d = \boldsymbol{H}_z(\gamma)\ddot{\boldsymbol{x}}_d \end{aligned} \tag{12}$$

where $x_t,\ y_t$ represent the $2D$ components of $\boldsymbol{x}_t$, $a = 0.3$, $b = 4$ and $t_0 = 1$. Different directions of movement are achieved by transforming the goals with $\boldsymbol{H}_z(\gamma)$, which defines a rotation around the $\boldsymbol{z}$-axis of an angle γ.

Fig. 2 collects three instances of the simulated movement (along the $-\boldsymbol{x}$ direction, $\gamma = \pi$). The left diagram shows the feasible major and minor axes of the endpoint stiffness using scaled (scaling = 0.0006) ellipses (ellipses are omitted for visibility reasons). The ellipse is a common way to visualize the task stiffness (Flash and Mussa-Ivaldi, 1990; Cui et al., 2008), where the major axis (red) of the ellipse is oriented along the maximum stiffness and the area is proportional to the determinant of $\boldsymbol{K}_t$, conveying the stiffness amplitude. The stiffness capacity (area) is increased in the last pose, since the arm has already reached its final position and muscle forces are not needed for it to execute any further motion. The second diagram (middle) depicts the distribution of ellipse parameters (area and orientation ϕ). Finally, the rightmost box plot shows the feasible joint stiffness distribution at three distinct time instants. Experimental measurements (Perreault et al., 2001) have showed that the orientation of stiffness ellipses varies in a range of about 30°. While our simulation results confirm this, they also reveal a tendency of fixation towards specific directions for higher stiffness amplitudes. The large variation of feasible stiffness verifies that this type of analysis conveys important findings that complement experimental observations.

3.2. Calculation of the feasible joint stiffness during walking

This experiment involves a model available in the `OpenSim` repository, used to estimate the joint stiffness during walking. The model has ten DoFs and a reduced set of eighteen Hill-type muscles (Millard et al., 2013) that are important for gait. The model was first scaled using a static pose in order to match the subject-specific anthropometrics. Afterwards, IK and ID were performed to obtain the kinematics and kinetics required to track the experimental marker trajectories and match the ground reaction forces.

Recall that in the definition of joint stiffness (Eq. (5)) the muscle moment arm must be differentiated with respect to the generalized coordinates. Unfortunately, `OpenSim` lacks the analytical means for evaluating higher order derivatives, as it computes the muscle moment arm numerically from the input joint configuration. In order to derive a symbolic representation, multivariate polynomial fitting (van den Bogert et al., 2011) was performed on samples of the muscle moment arm at different configurations. To reduce the complexity and improve the robustness of the fit, we determined the coordinates affecting each element in the moment arm matrix, by identifying the DoFs spanned by each muscle. Fig. 3 compares the sampled and symbolically obtained moment arm of the vastus intermedius (a mono-articular muscle) at the knee joint as a function of the knee flexion angle and the moment arm of the hamstring muscle at the knee joint as a function of the hip and knee flexion angles.

The feasible muscle force set was computed at each time step of the analysis, using Eqs. (9) and (10), assuming a linear muscle model. The short range stiffness (Eq. (4)) was used to form the muscle stiffness diagonal matrix $\boldsymbol{K}_m$.

Fig. 4 depicts the feasible joint stiffness of the hip, knee and ankle joints during walking with the heel strike and toe-off events annotated accordingly. These results confirm experimental measurements (Shamaei et al., 2015) and furthermore present similarities in the outline of the minimum stiffness predicted by our method. Notably, the hip stiffness range is gradually decreasing between heel strike and toe-off, because the flexor muscles are preparing for the swing phase and the capacity to increase the joint stiffness reaches its lowest value before the toe-off event. A similar pattern is observed at the knee joint, which undergoes a flexion and a subsequent extension during the swing phase. We observe that the capacity of the muscles to modulate the ankle stiffness is not decreased and the range is gradually shifted upwards in the region between the heel strike and toe-off events. The increase in the minimum possible values of the ankle stiffness is attributed to the counterbalance of the ground reaction forces by the ankle plantar flexion muscles. As muscle effort is spent by these muscles, one would expect a lower maximum bound, which is not the case here. This could be contributed to the fact that the musculoskeletal system is asymmetric, i.e., the plantar flexion muscles can induce larger magnitudes of moment at the ankle joint in comparison to the dorsiflexion muscles. We can conclude that the contribution of the ground reaction forces results in an increase of the ankle stiffness.

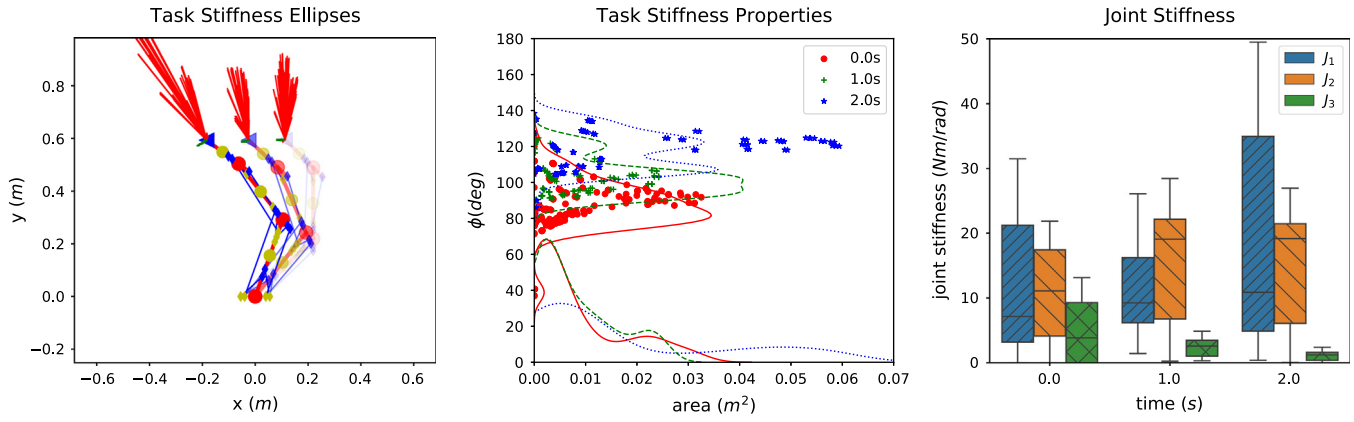

Fig. 2. Collected results of the simulated arm movement (along the $-\boldsymbol{x}$ direction, $\gamma = \pi$) at three time instants. Left diagram shows the feasible endpoint stiffness using scaled ellipses (scaling = 0.0006), where the red and green lines denote the major and minor axes, respectively. The middle plot illustrates the ellipse parameter distribution (area and orientation ϕ). The box plot on the right depicts the feasible joint stiffness distribution. (For interpretation of the references to color in this figure legend, the reader is referred to the web version of this article.)

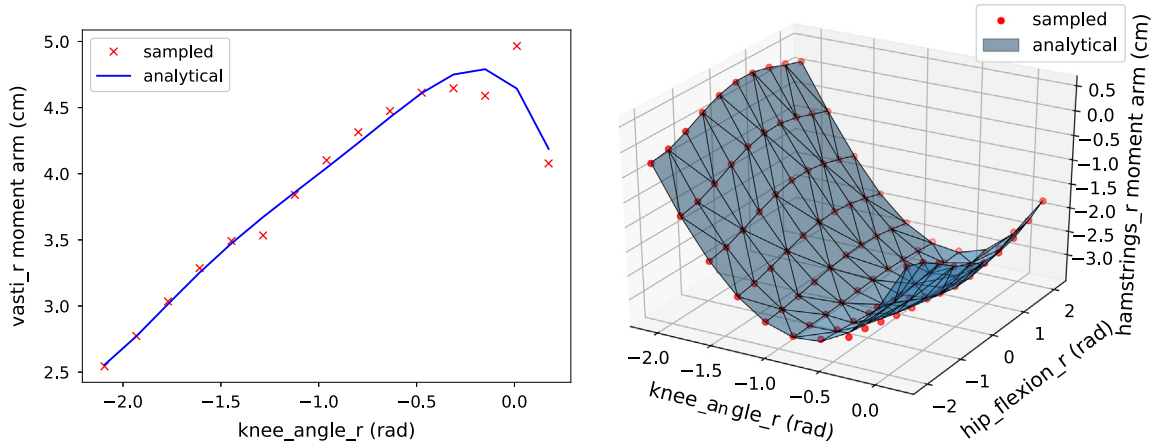

Fig. 3. Comparison between the sampled and symbolically obtained moment arm of the vastus intermedius muscle at the knee joint as a function of the knee flexion angle (left). Likewise, the moment arm of the hamstring muscle at the knee joint as a function of the hip and knee flexion angles (right).

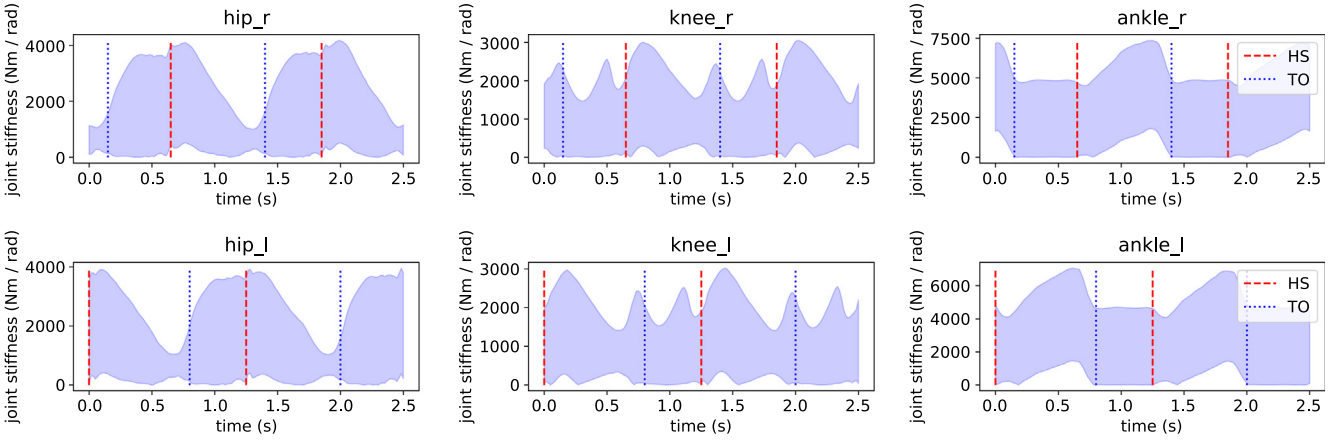

Fig. 4. The feasible joint stiffness of the hip, knee and ankle joints during walking with the heel strike (HS) and toe-off (TO) events annotated accordingly.

4. Discussion

The evaluation of task and joint stiffness is important because the CNS does not coordinate the motion of the limbs alone, but also regulates the overall stability, impedance and admittance of the musculoskeletal system. As musculoskeletal systems are intrinsically redundant, it is very difficult to interpret the hierarchical muscle activation patterns, especially when different muscle groups are co-activated. Considering these facts, we show that global stiffness evaluation is possible, hence this metric can be used to characterize various actions and complement traditional analyses. The calculation of the feasible stiffness can aid in finding patterns of low stiffness capacity in order to improve the design of products and interventions that target these aspects of movement (e.g., exoskeleton design, interaction with the environment, ergonomics, etc.). Moreover, this kind of analysis can be used in combination with the single solution methods in order to evaluate the uncertainty in the estimated quantities due to redundancy.

An accurate estimation of muscle forces is necessary for the assessment of the stiffness. Since measuring muscle activity poses many challenges and model-based estimation relies on assumptions that may not hold, a more holistic approach was adopted in this study. Feasibility studies have been successfully translated into clinical practice (Valero-Cuevas, 2009; Kutch and Valero-Cuevas, 2011; Valero-Cuevas et al., 2015) and their potential was explored here in the context of the feasible stiffness computation. The main advantage of the proposed approach is that the feasible muscle forces are action-specific, accounting for the dynamic evolution of the motion, while also satisfying the physiological constraints of the muscles, outlining the various factors that affect the solution space. Another important advantage of this formulation is that different muscle models, including nonlinear Hill-type and muscle synergies, can be used in the derivation of the feasible inequality. The bottleneck of this method lies in the time complexity of the vertex enumeration algorithm, used for sampling the feasible space satisfying the constraints presented as linear inequalities. Given that the space defined by the inequality in Eq. (9) is convex and bounded (Supplementary materials), the complexity is cubic ($O(m^3)$) with respect to the number of muscles. In highly complicated musculoskeletal models with a large number of muscles, the aforementioned deterministic approach becomes computationally intractable due to the cubic time complexity growth. In such cases, randomized algorithms have to be employed to provide a representative sampling of the high-dimensional polytope (Vempala, 2005).

While task and joint stiffness can be measured experimentally using specialized equipment, one cannot estimate the muscle stiffness from those measurements alone, because the mapping from low- (task or joint) to high-dimensional muscle stiffness is not unique. Therefore, accurate estimation of muscle stiffness from

task or joint stiffness is in general not possible, whereas validation would require direct measurement. Consequently, identification of the feasible solution space, as outlined in this work, can help to properly interpret results obtained from the redundant musculoskeletal systems.

The presented studies demonstrate the application of the proposed methodology in the context of real-world tasks. The first used a simplified model to study the arm endpoint stiffness, while the second used a more realistic `OpenSim` gait model to examine the joint stiffness during walking. The main weakness of the proposed method is that the accuracy in the predicted quantities depends on the quality of the musculoskeletal model that is being used, thus it is important to examine the sensitivity of the feasible stiffness with respect to the uncertainties in the model parameters. Nevertheless, the obtained results confirm previous findings and outline the feasible solution space, emphasizing that misinterpretation due to large variability is possible if the null space solutions are ignored. The analysis provides useful conclusions and insights, such as the balance between stiffness capacity and task requirements, indicating that higher task requirements reduce the ability for stiffness modulation.

5. Conclusion

In this study, we presented a method to determine the feasible task and joint stiffness of the musculoskeletal system for any movement. Undoubtedly, this is crucial for understanding the muscle coordination mechanisms and the various strategies available to the CNS, aiding in the development of effective evaluation and treatment of disorders such as Parkinson's disease. Practical and experimental limitations severely hinder the in vivo measurement of stiffness, while model-based estimation suffers from the musculoskeletal redundancy. To overcome the latter limitation, we choose to model the muscle redundancy using the notion of null space and identify the possible solutions that satisfy the task and muscle constraints. Results show that the musculoskeletal system is capable of achieving a highly variable stiffness using muscle co-contraction, highlighting the importance of performing feasibility studies.

Conflict of interest

None of the authors had any conflict of interest regarding this manuscript.

Acknowledgment

The authors would like to thank Aristotelis Spathis-Papadiotis for his valuable remarks and countless discussions on these topics. Other acknowledgments are owed to Dr. Evangelia Zacharaki for her comments on the manuscript. This work was supported by the EC Horizon 2020 project OACTIVE Grant Agreement No. 777159 and by the EC FP7 project NoTremor Grant Agreement No. 610391. There was no additional external funding received for this study. The funders had no role in the study design, data collection and analysis, decision to publish, or preparation of the manuscript.

Appendix A. Supplementary material

Implementation details and detailed derivation can be found in the supplementary materials. Supplementary data associated with this article can be found, in the online version, at https://doi.org/10.1016/j.jbiomech.2019.01.017.

References

Anderson, F.C., Pandy, M.G., 2001. Static and dynamic optimization solutions for gait are practically equivalent. J. Biomech. 34, 153–161. https://doi.org/10.1016/S0021-9290(00)00155-X. Available from: arXiv:154.

Avis, D., Fukuda, K., 1992. A pivoting algorithm for convex hulls and vertex enumeration of arrangements and polyhedra. Discret. Comput. Geom. 8, 295–313. https://doi.org/10.1007/BF02293050.

Babikian, S., Valero-cuevas, F.J., Kanso, E., 2015. Bio-inspired actuation of slow movements. J. Nonlinear Sci., 1–12 https://doi.org/10.1007/s00332-016-9305-x.

Bernshtein, N.A., 1967. The Co-Ordination and Regulation of Movements. Pergamon Press, Oxford.

van den Bogert, A.J., Blana, D., Heinrich, D., 2011. Implicit methods for efficient musculoskeletal simulation and optimal control. Proc. IUTAM 2, 297–316. https://doi.org/10.1016/j.piutam.2011.04.027 <http://www.sciencedirect.com/science/article/pii/S2210983811000289> .

Cui, L., Perreault, E.J., Mass, H., Sandercock, T., 2008. Modeling short-range stiffness of feline lower hindlimb muscles. J. Biomech. 41, 1945–1952. https://doi.org/10.3174/ajnr.A1256.Functional. Available from: arXiv:NIHMS150003.

Delp, S.L., Anderson, F.C., Arnold, A.S., Loan, P.L., Habib, A., John, C.T. . . .Thelen, D.G., 2007. OpenSim: open-source software to create and analyze dynamic simulations of movement. IEEE Trans. Biomed. Eng. 54, 1940–1950.

Erdemir, A., McLean, S.G., Herzog, W., Van Den Bogert, A.J., 2007. Model-based estimation of muscle forces exerted during movements. Clin. Biomech. 22, 131–154. https://doi.org/10.1016/j.clinbiomech.2006.09.005 <http://www.ncbi.nlm.nih.gov/pubmed/17070969> .

Flash, T., 1987. The control of hand equilibrium trajectories in multi-joint arm movements. Biol. Cybern. 57, 257–274. https://doi.org/10.1007/BF00338819.

Flash, T., Hogan, N., 1985. The coordination of arm movements: an experimentally confirmed mathematical model. J. Neurosci. 5, 1688–1703. doi:4020415.

Flash, T., Mussa-Ivaldi, F.A., 1990. Human arm stiffness characteristics during the maintenance of posture. Exp. Brain Res. 82, 315–326. https://doi.org/10.1007/BF00231251 <http://www.ncbi.nlm.nih.gov/pubmed/2286234> .

Hogan, N., 1981. The mechanics of multi-joint posture and movement control. Biol. Cybern. 52, 315–331.

Hu, X., Murray, W.M., Perreault, E.J., 2011. Muscle short-range stiffness can be used to estimate the endpoint stiffness of the human arm. J. Neurophysiol. 105, 1633–1641. https://doi.org/10.1152/jn.00537.2010.

Inouye, J.M., Valero-Cuevas, F.J., 2016. Muscle synergies heavily influence the neural control of arm endpoint stiffness and energy consumption. PLoS Comput. Biol. 12, 1–24. https://doi.org/10.1371/journal.pcbi.1004737.

Khatib, O., Demircan, E., De Sapio, V., Sentis, L., Besier, T.F., Delp, S.L., 2009. Robotics-based synthesis of human motion. J. Physiol. 103, 211–219. https://doi.org/10.1016/j.jphysparis.2009.08.004 <http://linkinghub.elsevier.com/retrieve/pii/S092842570900045X> .

Koeppen, R., Sternad, D., Huber, M.E., Hogan, N., 2017. Controlling physical interactions: humans do not minimize muscle effort. In: Proc. ASME 2017 Dyn. Syst. Control Conf., pp. 1–8.

Kolda, T.G., Bader, B.W., 2009. Tensor decompositions and applications. SIAM Rev. 51, 455–500. https://doi.org/10.1137/07070111X. Available from: arXiv:1404.3905 <http://epubs.siam.org/doi/10.1137/07070111X> .

Kutch, J.J., Valero-Cuevas, F.J., 2011. Muscle redundancy does not imply robustness to muscle dysfunction. J. Biomech. 44, 1264–1270. https://doi.org/10.1016/j.jbiomech.2011.02.014.

Millard, M., Uchida, T., Seth, A., Delp, S.L., 2013. Flexing computational muscle: modeling and simulation of musculotendon dynamics. J. Biomech. Eng. 135, 1–12. https://doi.org/10.1115/1.4023390 <http://www.pubmedcentral.nih.gov/articlerender.fcgi?artid=3705831&tool=pmcentrez&rendertype=abstract> .

Mussa-Ivaldi, F.A., Hogan, N., Bizzi, E., 1985. Neural, mechanical, and geometrical factors subserving arm posture in humans. J. Neurosci. 5, 2732–2743. https://doi.org/10.1056/NEJM197706162962404.

Pedotti, A., Krishnan, V.V., Stark, L., 1978. Optimization of muscle-force sequencing in human locomotion. Math. Biosci. 38, 57–76. https://doi.org/10.1016/0025-5564(78)90018-4.

Perreault, E.J., Kirsch, R.F., Crago, P.E., 2001. Effects of voluntary force generation on the elastic components of endpoint stiffness. Exp. Brain Res. 141, 312–323. https://doi.org/10.1007/s002210100880.

Prilutsky, B.I., Zatsiorsky, V.M., 2002. Optimization-based models of muscle coordination. Exerc. Sport Sci. Rev. 30, 32–38. https://doi.org/10.1097/00003677-200201000-00007. Available from: arXiv:NIHMS150003.

Shamaei, K., Cenciarini, M., Adams, A.A., Gregorczyk, K.N., Schiffman, J.M., Dollar, A.M., 2015. Biomechanical effects of stiffness in parallel with the knee joint during walking. IEEE Trans. Biomed. Eng. 62, 2389–2401. https://doi.org/10.1109/TBME.2015.2428636.

Stanev, D., Moustakas, K., 2018. Simulation of constrained musculoskeletal systems in task space. IEEE Trans. Biomed. Eng. 65, 307–318. https://doi.org/10.1109/TBME.2017.2764630 <http://ieeexplore.ieee.org/document/8074739/> .

Stanev, D., Moustakas, K., 2019. Modeling musculoskeletal kinematic and dynamic redundancy using null space projection. PLoS One 14, 1–26. https://doi.org/10.1371/journal.pone.0209171.

Steele, K.M., Tresch, M.C., Perreault, E.J., 2015. Consequences of biomechanically constrained tasks in the design and interpretation of synergy analyses. J. Neurophysiol. 113, 2102–2113. https://doi.org/10.1152/jn.00769.2013 <http://www.ncbi.nlm.nih.gov/pubmed/25589591> .

Thelen, D.G., Anderson, F.C., 2006. Using computed muscle control to generate forward dynamic simulations of human walking from experimental data. J. Biomech. 39, 1107–1115. https://doi.org/10.1016/j.jbiomech.2005.02.010 <http://www.ncbi.nlm.nih.gov/pubmed/16023125> .

Valero-Cuevas, F.J., 2009. A mathematical approach to the mechanical capabilities of limbs and fingers. Adv. Exo. Med. Biol. 629, 619–633. https://doi.org/10.1007/978-0-387-77064-2 <http://link.springer.com/10.1007/978-0-387-77064-2> .

Valero-Cuevas, F.J., Cohn, B.A., Yngvason, H.F., Lawrence, E.L., 2015. Exploring the high-dimensional structure of muscle redundancy via subject-specific and generic musculoskeletal models. J. Biomech. 48, 2887–2896. https://doi.org/10.1016/j.jbiomech.2015.04.026.

Valero-Cuevas, F.J., Hoffmann, H., Kurse, M.U., Kutch, J.J., Theodorou, E.A., 2009. Computational models for neuromuscular function. IEEE Rev. Biomed. Eng. 2, 110–135. https://doi.org/10.1109/RBME.2009.2034981.Computational.

Vempala, S.S., 2005. Geometric random walks: a survey. MSRI Comb. Comput. Geom. 52, 573–612.

Wesseling, M., Derikx, L.C., de Groote, F., Bartels, W., Meyer, C., Verdonschot, N., Jonkers, I., 2015. Muscle optimization techniques impact the magnitude of calculated hip joint contact forces. J. Orthop. Res. 33, 430–438. https://doi.org/10.1002/jor.22769.